SSCL-227

SSCL-227

Superconducting Super Collider Laboratory

Energy Scaling of Low-Energy Neutron Yield, the e/π Ratio, and Hadronic Response in a Calorimeter

D. Groom
SSC Central Design Group

July 1989

SSC-227

ENERGY SCALING OF LOW-ENERGY NEUTRON YIELD, THE e/π RATIO, AND HADRONIC RESPONSE IN A CALORIMETER*

Don Groom
SSC Central Design Group†

July 1989

* Submitted to the Proceedings of the Workshop on Calorimetry for the Superconducting Supercollider, Tuscaloosa, AL, March 13–17, 1989.
† Operated by the Universitites Research Association for the U.S. Department of Energy

SSC-227
15 July 1989

Energy Scaling of Low-Energy Neutron Yield, the e/π Ratio, and Hadronic Response in a Calorimeter

Don Groom
SSC Central Design Group, LBL 90-4040, Berkeley CA 94720

In each early collision in a high-energy hadronic cascade about 1/3 of the energy goes into π^0's and is thereafter lost to hadronic interaction. As a result, the level of low-energy hadronic activity in an absorber (as measured by the total yield of $\approx$ 1 MeV neutrons, the total number of nuclear collisions above some cutoff energy, the response of a calorimeter when electromagnetic components are excluded, etc.) rises more slowly than linearly with energy. A naïve induction argument yields a power law dependence with an exponent m near 0.85. Simulations with a variety of codes corroborate this result for $E > 10$ GeV. To the extent that this functional form is valid, the ratio of a calorimeter's response to an incident electron to that for an incident hadron is

$$\frac{R_e}{R_h}\left(=\frac{e}{\pi}\right) = \frac{1}{1-(1-\epsilon_h/\epsilon_e)(E/E_0)^{m-1}} ,$$

where ϵ_e and ϵ_h are the calorimeter efficiencies for detecting low-energy electronic and hadronic energy deposition, respectively, and E_0 is a scale factor near 1 GeV. This one-parameter function (if we neglect the slight m dependence) provides a good fit to available test-beam data, and has the correct asymptotic behavior.

1. Introduction

In a high-energy hadron-induced cascade the number of secondaries increases very rapidly as the energies of the interacting particles decrease. In the first few generations π^0's are produced, "bleeding off" a substantial fraction of the energy into electromagnetic cascades. This fraction is sensitive to multiplicity fluctuations in a small number of interactions, and hence is subject to large fluctuations. At the end of the cascade particles finally give up their energy to ionization, nuclear excitation, spallation, fission, etc. Ionization losses by high-energy particles contributes only negligibly to the total energy deposition, and it is fair to say that essentially all of the signal detected by the sensitive part of a calorimeter is produced by low-energy particles.

Conversion of the deposited energy to signal is quite different for the electromagnetic and hadronic components. In the electromagnetic case almost all of the signal is from the ionization produced by electrons. These are close to minimum ionizing, and the signal is therefore not particularly subject to nonlinearities such as saturation effects. On the other hand, the hadronic debris (ionizing hadrons and spallation fragments) is highly ionizing, so that saturation effects are important in the conversion of energy loss to signal. Much of the energy does not show up as ionization at all (e.g. that carried in low-energy nuclear recoil), and a large fraction of the energy is carried by low-energy neutrons which take a long time to interact.

For our purposes it is sufficient to say that electromagnetic energy loss is converted to an electrical signal with efficiency ϵ_e. In the case of an incident photon

or electron, all of the energy is measured with this efficiency. In the case (incident hadron the energy of secondary π^0's is measured with efficiency ϵ_e, ' that of the "low-energy hadronic activity" is detected with a different efficienc This efficiency includes saturation effects, energy missed because of a finite time, etc. Most of the many physical mechanisms involved in hadron energy decrease the detection efficiency, so in most cases ϵ_h is less than ϵ_e. If the insens volume (the plate material) is thick and high-Z, electromagnetic showers de; a disproportionally small fraction of their energy in the sensitive volume, ar might be less than ϵ_h. If $\epsilon_e/\epsilon_h = 1$, the system is said to be compensated.

Fig. 1 shows the energy division of 1000 π^- cascades in lead, as simulated FLUKA87 [1]. As can be seen, the electromagnetic fraction varies between 20% 92%. The finite width of the band is due to (a) albedo losses, i.e. energy ca: by particles back-scattering out of the front face, and (b) energy not prop accounted for by the program. Moreover, the band is not quite at 45°; FLU itself has $\epsilon_e/\epsilon_h \approx 0.92$! If we add the two energies with $\epsilon_e/\epsilon_h = 1.00$, we ol the solid histogram in Fig. 2, which has a standard deviation of 1.9%. The energy tail may also be seen in Fig. 1; its origin is unclear. The dashed and dc histograms were obtained for $\epsilon_e/\epsilon_h = 1.20$ and 1.55, respectively. Both these va are for real calorimeters, discussed later in this report. Even in the absen sampling fluctuations or other contributions to the resolution of a real calorim the resolution has been degraded to $47\%/\sqrt{E}$ in the second case merely by lack of compensation.

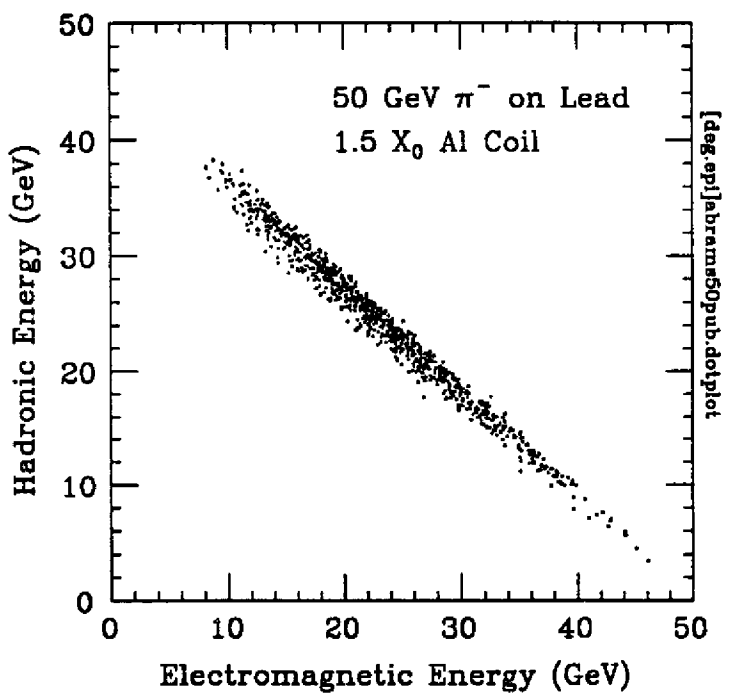

FIG. 1. The energy division of 1000 π^- cascades in lead, as simulated with FLUKA87. Here we define hadronic energy as total energy less electromagnetic, escaped, and missing energy. A thin aluminum plate on the front surface has little effect, and the dimensions are large enough that substantial energy can escape only from the front surface.

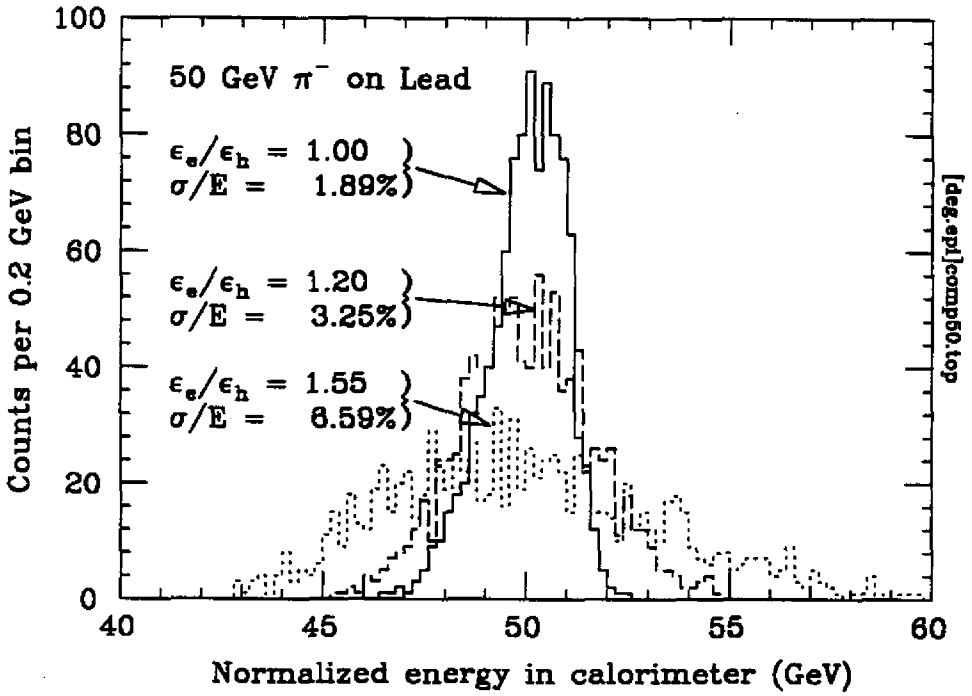

FIG. 2. The effect of lack of compensation on the resolution of an "ideal" calorimeter. The data of Fig. 1 are combined with different relative detection efficiencies for the hadronic and electromagnetic components. "Ideal" means that except for escaping energy and missing energy, everything is detected—there are no sampling effects, etc.

2. The universal low-energy hadron spectrum

A handful of high-energy secondary particles (mostly pions) and spallation products are produced in the first collision of a high-energy primary hadron incident on a calorimeter or other "beam stop." The spallation products often include protons and neutrons with substantial energy. The secondaries themselves undergo inelastic collisions, and the number of interactions ("stars") exponentiates as the energy degrades. Most of the activity, and in fact most of the energy deposition, occurs at low energies. In general, all information about the origin of the cascade is lost. Although the level of activity varies with the energy of the incident hadron, the energy distribution and relative importance of each hadronic species is independent of incident species or energy. This concept underlies much of the present discussion.

Of course this theorem is not quite true. A higher-energy primary is capable of producing more high-energy secondaries, but these have little weight in the total energy deposition. Moreover, the higher-energy secondaries and spallation nucleons tend to concentrate nearer the axis and nearer the beginning of the cascade, and a higher energy shower has greater longitudinal development. Only neutrons propagate to large radial distance from the shower core, and low-energy neutrons (below ~150 MeV) have a flatter radial distribution than do higher-energy components (see Appendix 17 of Ref. 2). None of these details have much to do with the observable signal in an actual calorimeter.

It matters very little if the medium is homogeneous (like a lead beam sto textured (like a calorimeter with alternating metal plates and sensitive mate as long as the mean free path of the particles carrying most of the energy is compared to segmentation dimensions.

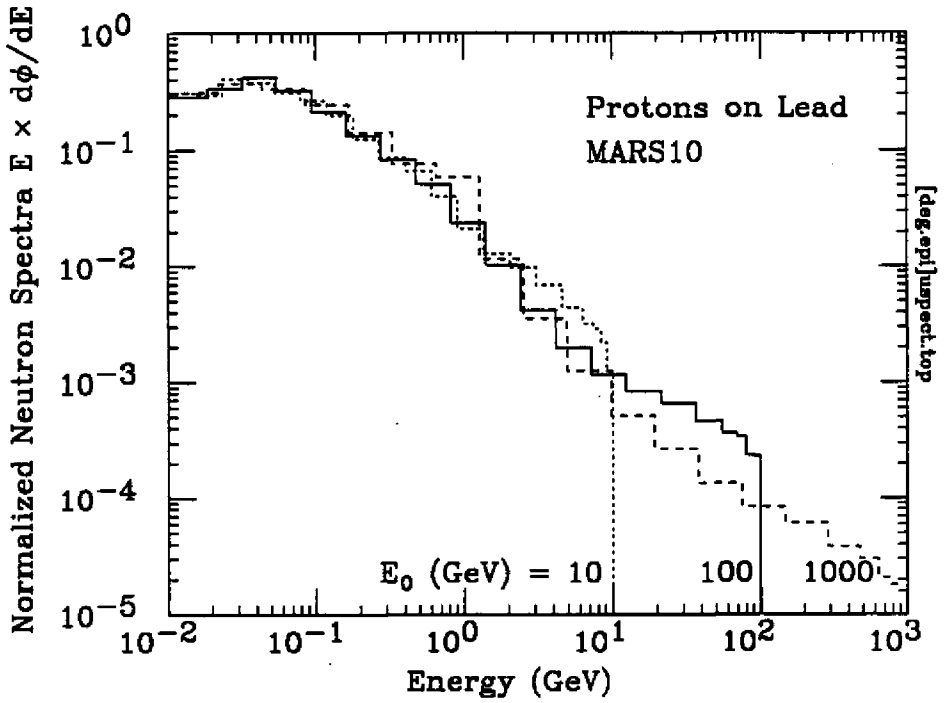

FIG. 3. Neutron spectra for different incident proton energies, as obtained by N. V Mokhov using MARS10 simulations. Normalization is adjusted to emphasize identity i shape below the beam energy cutoff.

The "universal spectrum" concept has been known for many years, m to people concerned with radiation shielding [3]. The results of a recent cal tion are shown in Figs. 3 and 4. Fig. 3 illustrates MARS10 simulations o neutron spectra (averaged over the cascade) produced by incident protons a 100, and 1000 GeV striking solid lead, all normalized for relative agreeme low energies [4, 5]. As can be seen, almost all of the particles have energies b 1 GeV, even for a 1 TeV incident beam, and the shapes of the spectra (b cutoff set by the incident beam energies) are identical within the accuracies o simulations.

Like other high-energy codes, MARS10 transports only "high-energy" p cles, down to an adjustable cutoff E_t at several tens of MeV. Below such ene nuclear physics effects become important. Lower-energy transport is usually dled by a separate code. The apparent turnover of the spectrum at 40 MeV (v $d\varphi/d(\ln E)$ is plotted as a function of $\ln E$) is therefore spurious. With pr transport to lower energies, the neutron spectrum shows a broad peak wit maximum just below 1 MeV, as is corroborated by experiment [6]. This fea is characteristic of all materials, although the exact position of the peak vari

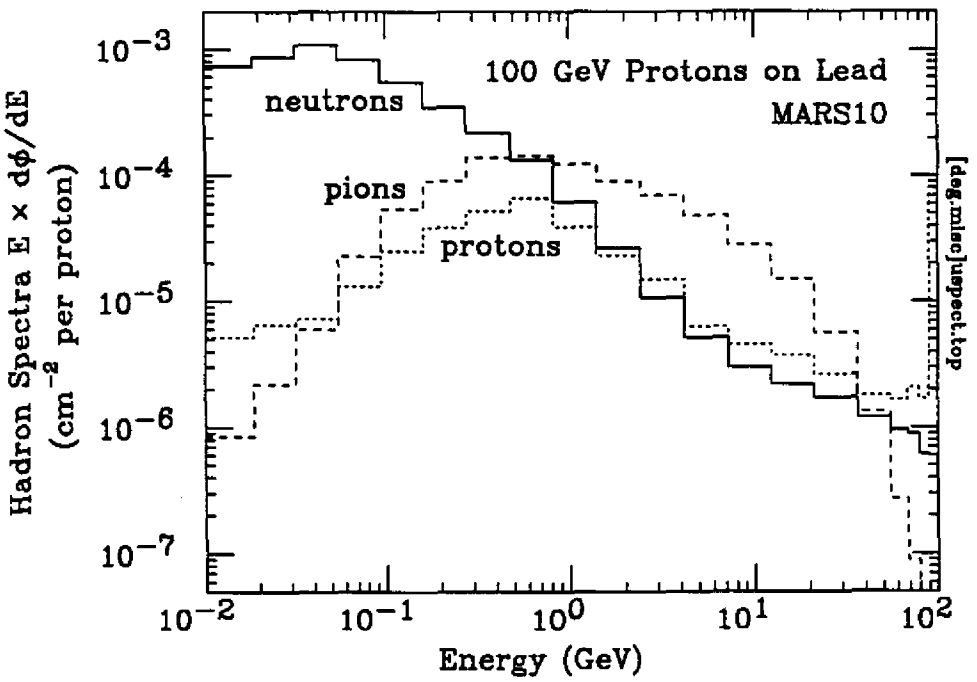

FIG. 4. Spectra of neutrons, protons, and charged pions in cascades induced by 100 GeV protons in lead, as calculated by N. V. Mokhov using MARS10.

little bit from material to material. About half of the total flux falls below 100 keV, with the exact fraction being strongly dependent upon the amount of low-Z material (hydrogen) which is present. This "thermal" component seems to have little radiological effect of any interest, but it may make other contributions to calorimeter response. For radiological purposes, "all the neutrons are at 1 MeV."

Fig. 4 shows spectra for the three significant hadronic species, this time for an incident proton energy of 100 MeV. As might be expected, the high-energy proton spectrum is about the same as that of neutrons. At low energies the protons quickly lose energy by ionization; they are nearly two orders of magnitude less important than neutrons at 100 MeV and vanish rapidly as the energy decreases. Charged pions have a similar behavior, but they are more abundant than nucleons at high energies.

3. "Low-energy hadronic activity"

There are many measures of "low-energy hadronic activity," all of which exhibit almost the same dependence on incident hadron energy. These include:

- The hadronic part of a calorimeter's response. While this is the measure of greatest present interest, it is difficult to actually separate the hadronic and electromagnetic response. The electromagnetic part is prompt, concentrated on the cascade axis, and a large part of it occurs in the vicinity of the first interaction.
- Total neutron yield. The number of neutrons produced in a cascade is not

a very well-defined concept, since neutrons are produced and absorb the cascade develops. Their energy spectrum degrades as time passes energy-, time- and position-dependent *flux* of neutrons is well-defined its product with some nuclear interaction cross section, e.g. the cross s for the production of ^{239}Np in uranium at a particular energy. The yield of ^{239}Np can be measured [7], and provides a good measure o energy hadronic activity.

- Number of nuclear interactions ("stars") produced in the absorber by rons whose energy exceeds some threshold E_t. Most such interactio induced by hadrons (usually neutrons) with energies not far above E_t the comparatively few interactions with $E > E_t$ contribute little to the This measure has the advantage of being tallied by the transport cod is readily available in simulations.
- Number of neutrons falling below the threshold E_t in the simulation. A the absolute number means very little, since it depends upon E_t and arbitrary factors, but it tracks the energy dependence and event-to- fluctuations.

Both the number of stars and the number of below-threshold neutrons me "fast" hadronic activity, so the factors relating their magnitudes to the observed in a calorimeter will also depend upon hydrogen content, fission sections, gate width, etc. We do not pretend to calculate them.

4. Energy dependence of low-energy hadronic activity

An oversimplified induction argument may be used to obtain the energ pendence of the low-energy hadronic activity. Let $N(E)$ be one of the measu this activity discussed above; to fix ideas let it be the average number of neu falling below E_t for an incident hadron of energy E. Consider another inc hadron with energy nE, where n is the mean multiplicity in a collision. hadron produced in the collision produces $N(E)$ low-energy neutrons—exce the fraction f_{π^0} of neutral pions, which contribute their energy to the electro netic channel. In other words,

$$N(nE) = (1 - f_{\pi^0})\, n\, N(E) \ .$$

(The assumption that all of the secondaries have the same energy is of c incorrect, as are the assumptions that n and f_{π^0} are independent of energ will return to these points later.) If we now further assume that this iter equation has a solution of the form

$$N(E) = K\, E^m$$

we immediately find

$$1 - m = \frac{\ln\left(1/(1 - f_{\pi^0})\right)}{\ln n} \ .$$

The power-law assumption is thus justified *a posteriori*, and is correct if the c

assumptions are justified.

As an example, for the choices $f_{\pi^0} = 1/3$ and $n = 20$ we find

$$m = 0.86 \ .$$

Doubling the multiplicity changes m to 0.89, and if $f_{\pi^0} = 1/4$ rather than 1/3, m increase from 0.86 to 0.90. It is difficult to find realistic parameters for which m falls outside the range 0.85 to 0.90.

This insensitivity also provides justification for the assumptions. The multiplicity increases with energy, but only logarithmically or as a soft power of the energy, so $\ln n$ varies extremely slowly. Similarly, $\ln(1 - f_{\pi^0})$ is very insensitive to the variation of f_{π^0}. The assumption that all secondaries have energy E/n is not crucial unless $\ln n$ or $\ln(1 - f_{\pi^0})$ varies rapidly.

It is useful to rephrase the conclusion: After each collision in a hadronic cascade, only $(1 - f_{\pi^0})$ of the energy is available (on the average) for the next generation. This factor is applied every time the energy increases by the multiplicity, which results in a power-law increase in low-energy activity with increasing energy of the incident hadron. While our assumptions are not strictly true, the very nature of the process leads at least to a power-law-like behavior.

The behavior has been checked with the aid of several programs. Results obtained with FLUKA86 [1] are shown in Figs. 5 and 6, where we show both the number of neutrons dropping below $E_t = 50$ MeV and the number of stars scored by the program. In neither case does the absolute amplitude mean anything; in fact, fewer neutrons and more stars are scored with iron than with either lead or uranium. The yields are divided by the incident energy, so the slope of a power law fit is $m - 1$ rather than m. Straight-line fits are drawn for $m = 0.86$.

The divergence of the results from a power-law fit for incident energies below 10 GeV should be noted. Our arguments are meant to apply only when there are several high-energy generations in the cascade, so this behavior is hardly surprising. Nor is it fully understood.

When these results are plotted after dividing by the nonelectromagnetic energy fraction in the cascade, the slope is essentially zero. This corroborates our assumption that the slope is due to π^0 production.

Similar calculations made with MARS10 by N. V. Mokhov are shown in Fig. 7, where below-threshold neutron yields are plotted for $E_t = 10$ MeV [4, 5]. The same slopes are obtained as with FLUKA87, but in this case there is no deviation from the power law behavior below 10 GeV.

T. A. Gabriel has made similar calculations using two versions of HETC [8, 9], which are shown in Fig. 8. The old version was known not to include π^0 production correctly, and yields $m = 0.99$ and $m = 0.93$ for uranium and iron, respectively. The new version (HETC87) yields $m = 0.85$ and $m = 0.82$ for the two cases, in accord with results obtained with other codes.

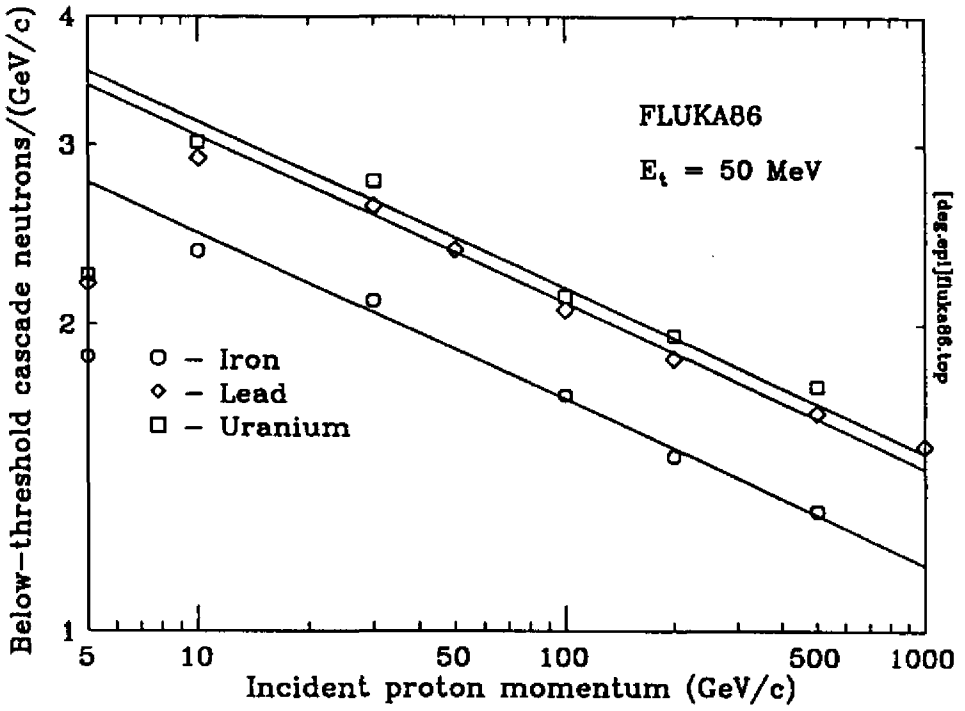

FIG. 5. The total number of cascade neutrons per unit incident momentum (energy) falling below a 50 MeV energy threshold as a function of incident hadron momentum, as simulated by FLUKA86. The solid lines have a slope of −0.14.

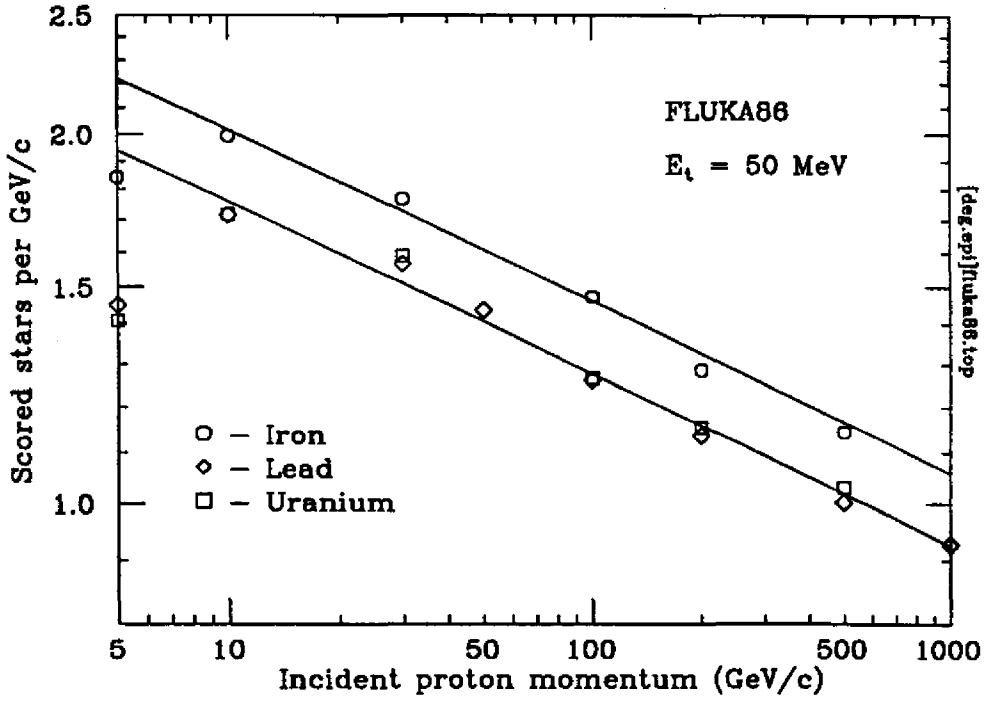

FIG. 6. The total number of nuclear interactions (stars) per unit incident momentum (energy) produced by hadrons with energy greater than 50 MeV as a function of incident hadron momentum, as simulated by FLUKA86. The solid lines have a slope of −0.14.

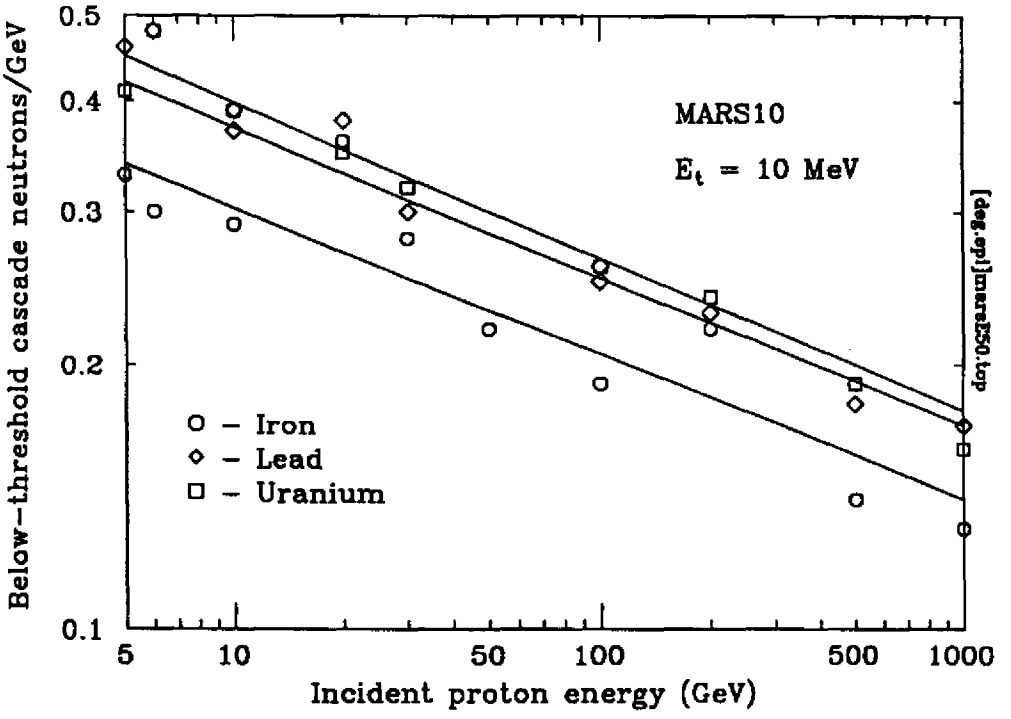

FIG. 7. The total number of cascade neutrons per unit incident energy falling below a 10 MeV energy threshold as a function of incident hadron momentum, as simulated with MARS10 by N. V. Mokhov. The solid lines have a slope of −0.14.

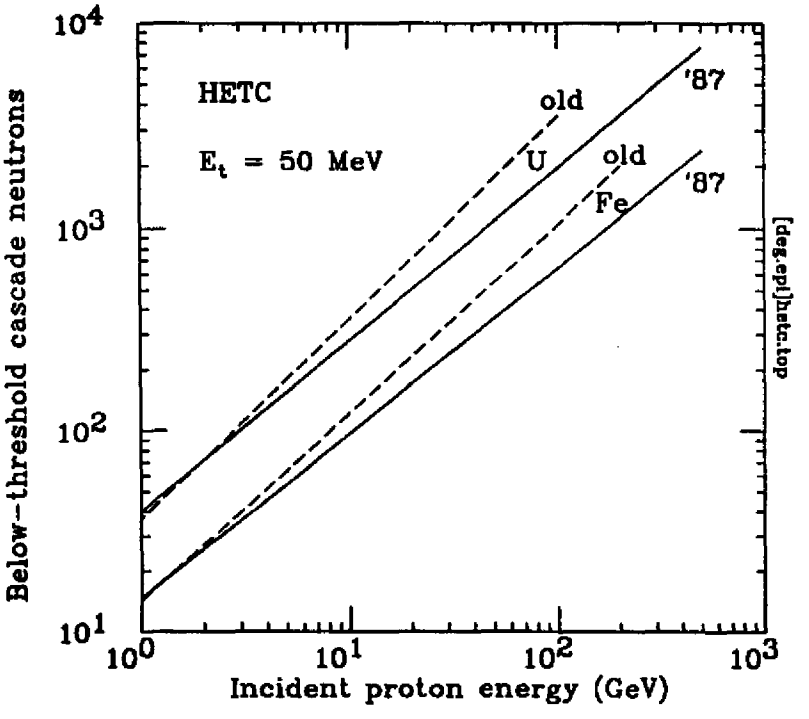

FIG. 8. The total number of cascade neutrons falling below a 50 MeV energy threshold as a function of incident hadron momentum, as simulated with HETC by T. A. Gabriel. The high-statistics data points are not shown. The dotted lines through the "old HETC" results have slopes of 0.99 and 0.93, respectively, and the solid lines obtained with the current version of the code have slopes of 0.85 and 0.82 for the two cases.

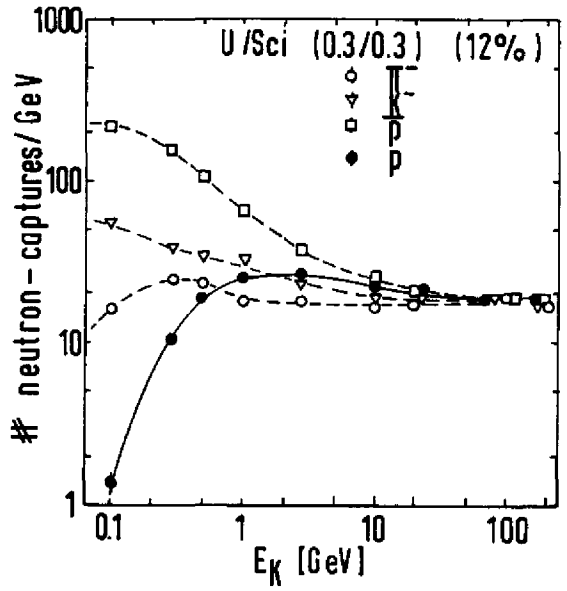

FIG. 9. The number of neutron captures per GeV of incident hadronic energy in a fine sampling uranium/scintillator calorimeter as a function of the kinetic energy of inciden hadrons. The figure is taken from Appendix 16 by H. Fesefeldt in Ref. 2.

Results obtained with GHEISHA [10] are a little more problematical. In F we reproduce Fig. 8 from Appendix 16 by H. Fesefeldt in Ref. 2. The numb neutron captures in a fine-sampling uranium/scintillator calorimeter per Ge incident energy is plotted as function of the kinetic energy of incident had The emphasis of the figure is upon differences at low energies, all of which be understood in terms of mass differences and annihilations. There is not r enough lever arm above 10 GeV to establish a slope, but the data would ap to be consistent with little or no π^0 production rather than with a slope in range $-0.10 > m - 1 > -0.15$.

5. The "e/π" ratio in calorimetry

In the above discussion we have distinguished between incident hadronic en that ends up in the electromagnetic channel from that which ends up as low-en hadronic activity. It is very nearly true that the response of a calorimeter to electromagnetic part of the energy (E_e) is proportional to that energy:

$$\text{Response} = \epsilon_e \, E_e$$

Similarly, the part of the signal due to low-energy hadronic activity is proporti to its energy E_h:

$$\text{Response} = \epsilon_h \, E_h$$

However, the physics producing ϵ_h is very different from that producing ϵ_e. T is a great deal of saturation because the ionization is by slow particles, energ lost to nuclear recoil and excitation, energy escapes from the system, electr

gates may have closed before all the energy has appeared, etc. All of these affect ϵ_h only, and there is no *a priori* reason to expect any particular value for the ratio ϵ_e/ϵ_h.* In the absence of preferential electromagnetic energy absorption in inactive regions, we might expect $\epsilon_e/\epsilon_h > 1$.

The total response of the calorimeter (in Coulombs, or Volts, or GeV) is just the sum of these contributions:

$$\begin{aligned} R_h &= \epsilon_h E_h + \epsilon_e E_e \\ &= \epsilon_h E_h + \epsilon_e (E - E_h) \ , \end{aligned} \tag{4}$$

where the total incident energy E is the sum of E_h and E_e.

In the above discussion we have established that $E_h \propto E^m$. It is convenient to introduce a scale factor E_0 so that we can write

$$\begin{aligned} E_h &= E_0(E/E_0)^m \\ &= E(E/E_0)^{m-1} \ . \end{aligned} \tag{5}$$

Substituting the second form for E_h in Eq. 4, we obtain

$$R_h = \epsilon_e E\big(1 - (1 - \epsilon_h/\epsilon_e)(E/E_0)^{m-1}\big) \ . \tag{6}$$

The response of the same calorimeter to an electron or photon is

$$R_e = \epsilon_e E \ , \tag{7}$$

and so the ratio of the electronic to hadronic responses is

$$\begin{aligned} \frac{R_e}{R_h}\left(= \frac{e}{\pi}\right) &= \frac{1}{1 - (1 - \epsilon_h/\epsilon_e)(E/E_0)^{m-1}} \\ &= \frac{1}{1 - a\,E^{m-1}} \ . \end{aligned} \tag{8}$$

The functional form given in Eq. 8 has two parameters, m and $a = (1 - \epsilon_h/\epsilon_e)\,E_0^{1-m}$. E_0 should be close to 1 GeV for physical reasons, but in any case only a can be obtained from experimental data. Representative examples of the function are shown in Fig. 10, where we list the more conventional ϵ_e/ϵ_h, under the assumption that $E_0 = 1$ GeV. In one case the effect of varying m is shown.

* ϵ_e/ϵ_h is "the intrinsic e/h" used by some authors.

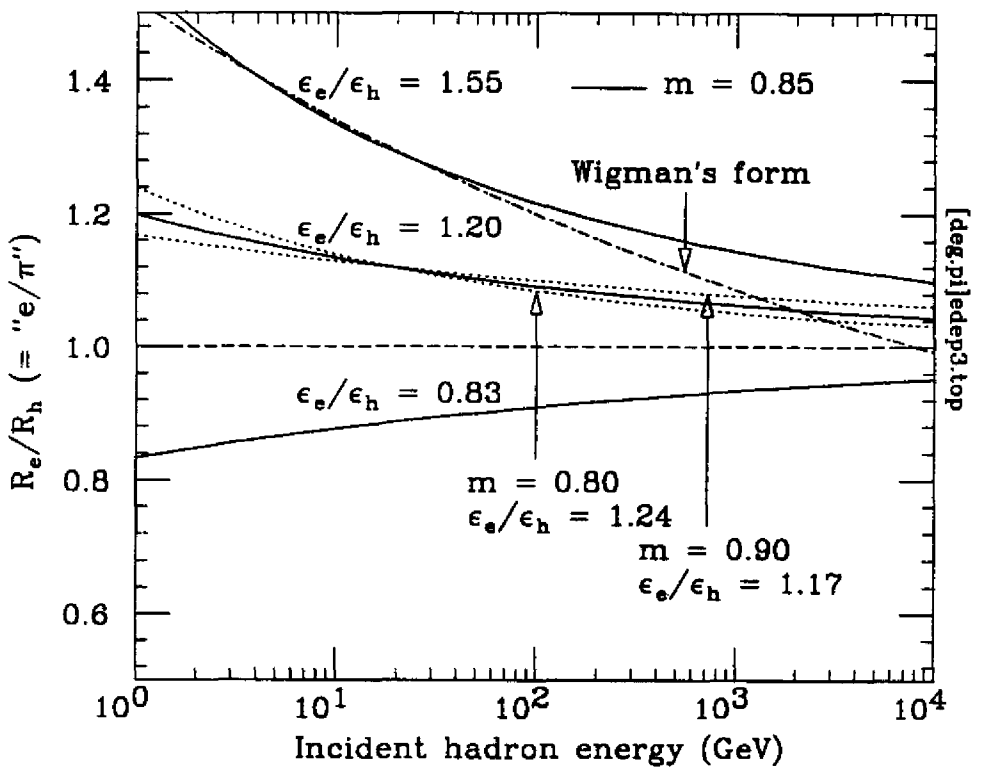

FIG. 10. The proposed function form for R_e/R_h (Eq. 8) for representative values of ϵ_e/ϵ taking $E_0 = 1$ GeV. Solid curves are for $m = 0.85$, while dotted curves are for $m = 0.$ and $m = 0.90$, with ϵ_h/ϵ_e adjusted for agreement with the $\epsilon_h/\epsilon_e = 1.20$, $m = 0.85$ ca at 20 GeV. Wigmans' form (Eq. 9) is shown by the dash-dotted curve for a case in whi agreement is forced for 1 GeV $< E_k <$ 100 GeV.

Wigmans has published a similar form[11]. If f is the fraction of the e of the incident hadron going into π^0's, then the equivalent of Eq. 4 becomes

$$R_h/E = f\epsilon_e + (1-f)\epsilon_h \ .$$

He further assumes

$$f = \kappa \ln E$$

(where $\langle\kappa\rangle \approx 0.1$ and E is in GeV) to obtain

$$\frac{R_e}{R_h}\left(=\frac{e}{\pi}\right) = \frac{\epsilon_e/\epsilon_h}{1-(1-\epsilon_e/\epsilon_h)\kappa\ln E} \ .$$

As can be seen from Fig. 10, this function is experimentally indistinguishable Eq. 8 over the region in which data is normally available. The main diffe is our weak negative power law dependence ($m - 1 \approx -0.15$) as compared Wigmans' logarithmic dependence. The electromagnetic fraction f can e: unity or become negative at reasonable energies. We believe that for phy reasons R_e/R_h must approach unity.

As many others have pointed out, because R_e is proportional to the incident electromagnetic energy the hadronic response of a calorimeter divided by the incident energy is just

$$R_h/E = \frac{k}{(R_h/R_e)} \ . \tag{10}$$

In other words, R_h is proportional to the reciprocal of the "e/π" ratio. This conclusion is independent of any particular model or parameterization, and says that unless ϵ_e/ϵ_h is unity a calorimeter has a nonlinear response to hadrons.

6. Comparisons with data

Three comparisons of Eq. 8 with data are made in this section. In all cases we have assumed $m = 0.85$ and adjusted a to obtain a reasonable fit.

The first is with CERN test-beam data obtained with an iron calorimeter. The data come from transparencies presented at a conference [12], so our information is somewhat fragmentary. R_e/R_h is shown in Fig. 11. The curve labeled "Wigmans" is of the form given in Eq. 9, with $(\epsilon_e/\epsilon_h)^{-1} = 0.659 \pm 0.005$ and $\kappa = 0.111 \pm 0.002$. The curve labeled "$a = 0.35$" is given by Eq. 8, with the parameter a chosen to give agreement with the data at 50 GeV. The two forms thus yield the same result for ϵ_h/ϵ_e if E_0 Eq. 8 is 1 GeV, as we have asserted, and corresponds to the top curve in Fig. 10.

Linearity data for this module is shown in Fig. 12. The functions shown are simply the reciprocals of those plotted in Fig. 11, scaled so that the response/GeV is unity at 80 GeV.

The second example is from test-beam results for the HELIOS uranium/liquid argon calorimeter [13].* The response ratio is shown in Fig. 13, with the fitting function parameters chosen to obtain agreement with data at 40 GeV; these correspond to $\epsilon_h/\epsilon_e = 1/1.20$ and $1/1.17$ for integration times of 100 ns and 250 ns, respectively, for $E_0 \approx 1$ GeV. We conclude that (a) no reasonable model will be able to incorporate the 400 GeV 250 ns point, and (b) there is no compelling evidence for a decrease in a with increasing gate time, even though such a decrease would be expected.

Finally, D0 test-beam results are shown in Fig. 14. In this case the data were read from the graph, and a simple least-squares adjustment of the parameter yielded $a = 0.051 \pm 0.015$, corresponding to $\epsilon_e/\epsilon_h = 1.054 \pm 0.017$ if E_0 is taken as 1 GeV. This near-compensation is consistent with the HELIOS results because a very long integration time ($\sim 2\ \mu$s) was used. In a study of a uranium/warm liquid system, Brau and Gabriel found that for 5 GeV incident protons only 85% of the visible energy had been deposited after 250 ns [15]. If we take the fit to the 250 ns HELIOS data at face value and assume that a similar fraction of the

* These preliminary data have been widely circulated. Note that the shorter integration time has been corrected to 100 ns on the advice of the authors.

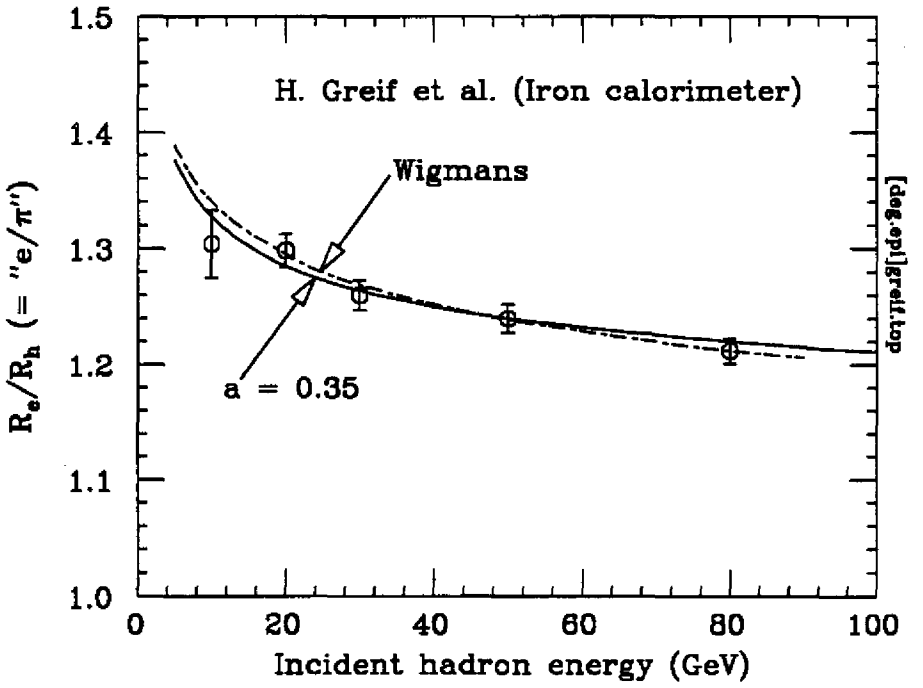

FIG. 11. Hadron response divided by electron response for an iron-plate calorimeter te module, as reported by H. Greif. Fits to the data are discussed in the text.

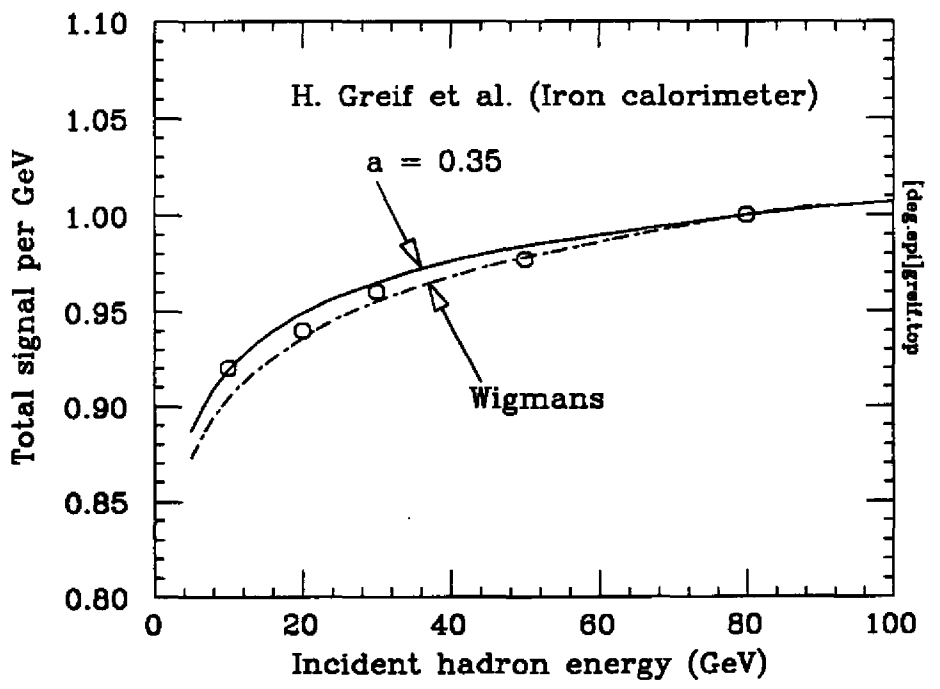

FIG. 12. Hadron linearity of the same iron-plate calorimeter module. Within a scal factor, the fits shown are the reciprocals of those given in Fig. 11.

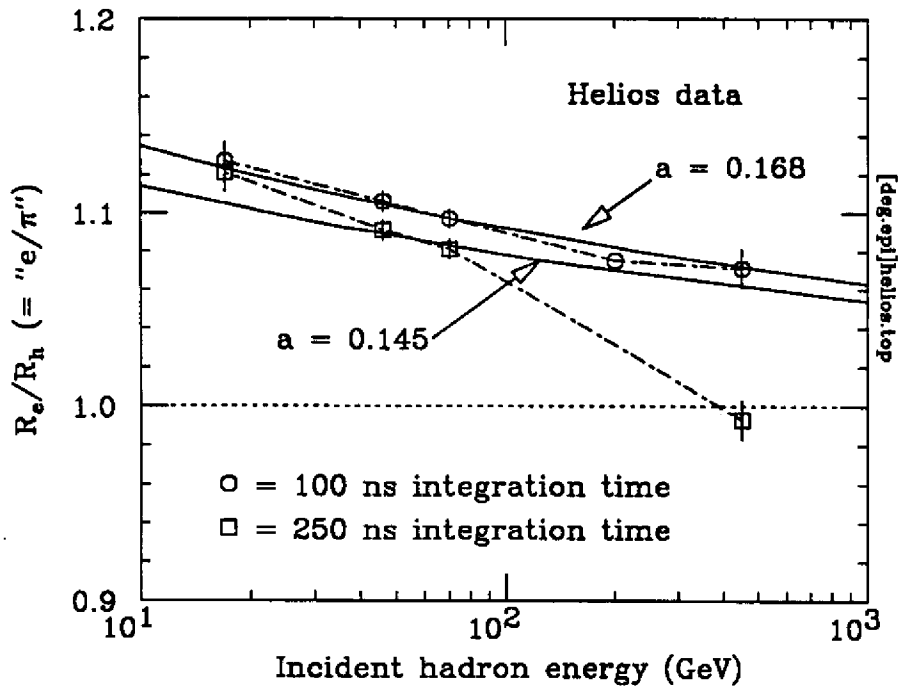

FIG. 13. Compensation data for a HELIOS uranium/liquid argon calorimeter test module. Curve parameters are chosen to obtain agreement with the 46 GeV data.

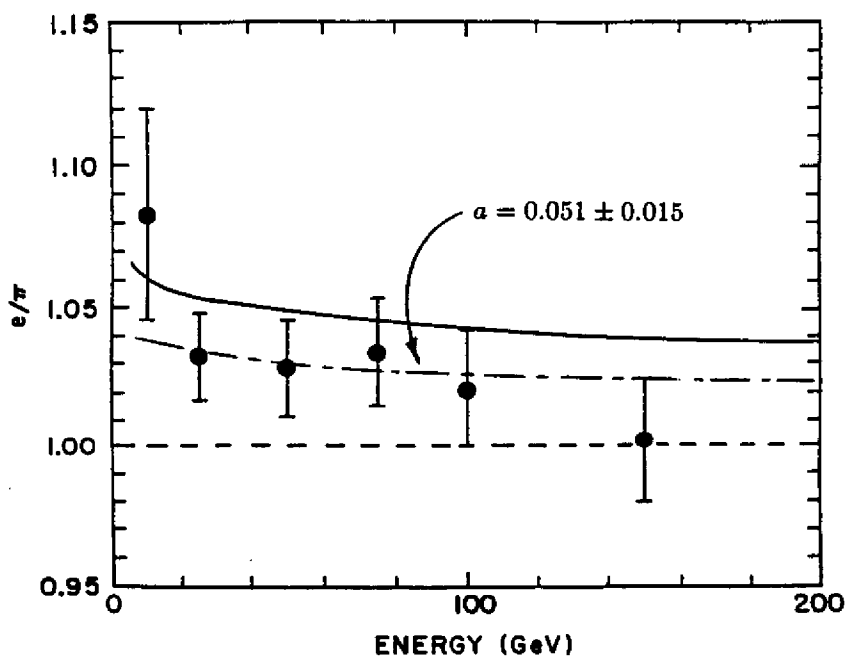

FIG. 14. Test-beam compensation data for a D0 uranium/liquid argon calorimeter module. A least-squares fit yields $a = 0.051 \pm 0.015$, or $\epsilon_e/\epsilon_h = 1.054 \pm 0.017$ if E_0 is taken as 1 GeV.

energy is yet to appear in uranium/liquid argon, we find that more or less co: compensation should occur for integration times of several microseconds, in with the D0 result.

7. Low-energy behavior

The region between 1 GeV and 10 GeV remains problematical. For one we must distinguish between momentum, total energy, and kinetic energy, a the possible contribution of annihilation energy. More seriously, the simu programs disagree: In FLUKA87 the low-energy hadronic activity per in GeV drops dramatically with decreasing energy in this region, while in M simulations it does not. If the yield drops we should expect R_h/E to decre R_e/R_h to increase sharply as the incident energy decreases from 10 GeV to There is some evidence that this occurs, and in any case this region will p welcome verification for the simulation programs.

8. Conclusions

To the extent that Eq. 8 provides a reliable description of the energy dence of R_e/R_h, one measurement suffices to determine the one sensitive p eter. This has significant consequences for future test beam work on calori Since most of the information comes at low energies (a few tens of GeV), th of high-energy test-beams for many calorimeter studies is minimal.

Further Monte Carlo work is needed, particularly at energies below 10

It might be conjectured that the fragmentation in the first hadron-n collision is not very different than that when a jet is produced. To the exten this is so, the response of a large, uniform calorimeter to an incident jet is the as its response to a hadron of the same energy. There are obvious differences as the greater penetration and presence of leading particles in the cascade in by a single hadron, but these have little to do with the total response.

9. Acknowledgments

Spirited discussions with G. R. Stevenson and J. S. Russ have contribu great deal to this paper. I am also indebted to R. Wigmans for important d sions about Eq. 9, and to N. V. Mokhov and T. A. Gabriel for both calcul and discussions.

10. References

1. P. A. Aarnio, A. Fassò, H-J. Möhring, J. Ranft and G. R. Stevenson, "FLUKA86 Guide," CERN TIS-RP/168 (1986);
   P. A. Aarnio, A. Fassò, J. Lindgren, J. Ranft and G. R. Stevenson, "Enhancements FLUKA86 Program (FLUKA87)," CERN TIS-RP/190 (1987).
2. "Radiation Levels in the SSC Interaction Regions," D. E. Groom, editor, SSC Central Group Report SSC-SR-1033 (June 1988).
3. T. A. Gabriel and R. T. Santoro, "Calculation of the Long-Lived Activity in Soil Pro by 500 GeV Protons," Oak Ridge National Laboratory Report ORNL-TM-3262 (1970)

4. N. V. Mokhov, J. D. Cossairt. Nucl. Instrum. Methods, A244, 349 (1986);
N. V. Mokhov, Soviet J. Particles and Nuclei, (Sept.-Oct. 1987), pp. 408-426;
N. V. Mokhov, "The MARS10 Code System: Inclusive Simulation of Hadronic and Electromagnetic Cascades and Muon Transport," Fermilab Report FN-509 (20 March 1989).
5. N. V. Mokhov, private communication (1988).
6. T. A. Gabriel, F. S. Alsmiller, R. G. Alsmiller, Jr., B. L Bishop, O. W. Hermann, and D. E. Groom, "Preliminary Simulation of the Neutron Flux Levels in the Fermilab Tunnel and Proposed SSC Tunnel," SSC Central Design Group Report SSC-110 (1987).
7. C. Leroy, Y. Sirios, and R. Wigmans, Nucl. Instrum. Meth. **A252**, 4 (1986).
8. R. G. Alsmiller, Jr. *et al.*, "Modifications of the High Energy Transport Code (HETC) and Comparisons with Experimental Results," presented at the ANS Topical Conference on Theory and Practices in Radiation Protection and Shielding, 22-24 April 1987, Knoxville, Tennessee; K. C. Chandler and T. W. Armstrong, "Operating Instructions for the High-Energy Nucleon-Meson Transport Code HETC," Oak Ridge National Laboratory Report ORNL-4744 (1972)
9. T. A. Gabriel, private communication (1988).
10. H. Fesefeldt, "The Physics of Hadronic Showers," RWTH Aachen PITHA 85/02 (1985).
11. R. Wigmans, Nucl. Instrum. Meth. **A265**, 275 (1988).
12. H. Greif, Viewgraphs from the International Workshop on Calorimeter Simulation, KFA Jülich, Germany (October 11-13, 1988).
13. H. Gordon, private communication (12 May 1989).
14. M. Abolins *et al.*, Fermilab preprint FERMILAB-Pub-89/38-E (February 1989) (to be published in Nucl. Instrum. Meth. A).
15. J. E. Brau and T. A. Gabriel, Oak Ridge National Laboratory Report ORNL/TM-10903 (January 1989).